UNIVERSITY OF BIRMINGHAM
University of Birmingham Research at Birmingham

Reaction kinetics of vanillin hydrodeoxygenation in acidic and nonacidic environments using bimetallic PdRh/Al2O3 catalyst

Aliu, Elias; Hart, Abarasi; Wood, Joe

DOI:
10.1021/acs.energyfuels.9b02993

License:
Creative Commons: Attribution (CC BY)

Document Version
Publisher's PDF, also known as Version of record

Citation for published version (Harvard):
Aliu, E, Hart, A & Wood, J 2019, 'Reaction kinetics of vanillin hydrodeoxygenation in acidic and nonacidic environments using bimetallic PdRh/Al_2O_3 catalyst', *Energy & Fuels*, vol. 33, no. 11, pp. 11712-11723. https://doi.org/10.1021/acs.energyfuels.9b02993

Link to publication on Research at Birmingham portal

General rights
Unless a licence is specified above, all rights (including copyright and moral rights) in this document are retained by the authors and/or the copyright holders. The express permission of the copyright holder must be obtained for any use of this material other than for purposes permitted by law.

•Users may freely distribute the URL that is used to identify this publication.
•Users may download and/or print one copy of the publication from the University of Birmingham research portal for the purpose of private study or non-commercial research.
•User may use extracts from the document in line with the concept of 'fair dealing' under the Copyright, Designs and Patents Act 1988 (?)
•Users may not further distribute the material nor use it for the purposes of commercial gain.

Where a licence is displayed above, please note the terms and conditions of the licence govern your use of this document.

When citing, please reference the published version.

Take down policy
While the University of Birmingham exercises care and attention in making items available there are rare occasions when an item has been uploaded in error or has been deemed to be commercially or otherwise sensitive.

If you believe that this is the case for this document, please contact UBIRA@lists.bham.ac.uk providing details and we will remove access to the work immediately and investigate.

Download date: 04. May. 2023

This is an open access article published under a Creative Commons Attribution (CC-BY) License, which permits unrestricted use, distribution and reproduction in any medium, provided the author and source are cited.

energy&fuels

Article

Cite This: Energy Fuels 2019, 33, 11712−11723

pubs.acs.org/EF

Reaction Kinetics of Vanillin Hydrodeoxygenation in Acidic and Nonacidic Environments Using Bimetallic PdRh/Al_2O_3 Catalyst

Elias Aliu, Abarasi Hart, and Joseph Wood*

School of Chemical Engineering, University of Birmingham, Edgbaston, Birmingham B15 2TT, United Kingdom

Supporting Information

ABSTRACT: The kinetics of hydrodeoxygenation (HDO) reaction in literature are mostly reported for single model compounds in bio-oil. However, these kinetic models may become invalid in the real bio-oil environment where other model compounds are present. This study investigates the effect of acetic acid, which is a major compound in bio-oil, on the liquid-phase HDO reaction kinetics of vanillin (VL). A synthesized bimetallic catalyst (PdRh/Al_2O_3) was utilized in a batch reactor at 308−328 K, 1−4 MPa H_2 gas partial pressure (P_H), 263−526 mM initial VL concentration (C_{VL0}), and 1.9−4.6 kg/m^3 catalyst loading with ethyl acetate as the reaction solvent. N_2 adsorption−desorption, scanning electron microscopy (SEM), X-ray diffraction (XRD), X-ray fluorescence (XRF), CO chemisorption, and mercury porosimetry methods were used to determine the physicochemical properties of the catalyst. Transport limitations in the system were ruled out via the Madon−Boudart test, Weisz−Prater criterion, agitation, and particle size test. In vanillin-only and vanillin−acetic acid environments, nonfirst-order dependence on P_H and C_{VL0} was found. Notably, lower reaction rates were observed in the presence of acetic acid compared to vanillin-only environment. Kinetic data for the vanillin-only and vanillin−acetic acid environments were successfully modeled using derived expressions from Langmuir−Hinshelwood−Hougen−Watson approach under the assumption of competitive dissociative hydrogen adsorption. The estimated activation energy for VL HDO reaction was 24.1 kJ/mol in vanillin-only environment and 51.0 kJ/mol in the presence of acetic acid.

1. INTRODUCTION

The world energy consumption is expected to grow by 20−30% from 2019 to 2040 as a result of the increase in population and rapid development in countries like China and India.[1] Conversely, the volume of fossil fuels accessible from reserves around the world has steeply declined over the past decade.[2,3] This disturbing trend in capacity of world fossil reserves and growing concern on the impact fossil fuels consumption has on the environment motivates the development of alternative renewable and sustainable energy sources.[4−6] Renewable sources of energy such as wind, solar, and hydrogen fuel cell are attractive substitutes for fossil resources. However, most of the existing infrastructure in the world works on liquid hydrocarbon fuels.[7,8] Hence, to utilize the above listed renewable energy sources, drastic changes will be required, necessitating a long duration until they are fully realized. At the moment, plant biomass is the only renewable and sustainable carbon source for producing liquid hydrocarbon fuel, otherwise known as bio-oil.[9−12] Consequently, production of bio-oil from plant biomass has increasingly become the subject of interest in energy research studies. Fast pyrolysis (FP) is the preferred technology for producing bio-oil because it requires lower costs compared to competing technology like liquefaction.[9,13−15] FP involves rapid heating of biomass to a temperature around 923 K in the absence of air.[16−19] Bio-oils produced via FP usually contain a significant amount of highly unstable oxygenated compounds such as aldehydes, ketones, carboxylic acids, guaiacols, cresols, syringols, and anisoles.[20−23] The fast processing conditions used in the production of bio-oil via FP are primarily responsible for the thermodynamic instability of these oxygenated compounds, which adversely affects the fuel quality. For instance, bio-oils have low pH, poor volatility, lower energy density, and high viscosity.[13,24−27] Fortunately, the fuel quality of bio-oil can be improved through a hydrotreating process known as hydrodeoxygenation (HDO).[19,28−35] However, the complexity of HDO processes and bio-oils makes it difficult to collect kinetic data for reactor sizing and overall process-optimization purposes. Most research studies on HDO are based on individual model compounds found in bio-oil to simplify the reaction and gain better understanding of the steps involved in the transformation process.[36−40] However, in the presence of other model compounds, the established kinetic relationship from single model compound studies may become invalid. Lignin-derived phenolics containing multiple functional groups such as cresols, guaiacols, and anisoles are commonly used as model compounds in HDO reactions.[37,41] In this work vanillin, a lignin-derived phenolic compound with three functional groups (ether, hydroxyl, and aldehyde), is selected because it has been reported in more than four different analytical studies as a component of real bio-oil but is less reported as a model compound for HDO.[42−46] Sulfided transition metals, which include cobalt molybdenum (CoMo) and nickel molybdenum (NiMo) on conventional support such as alumina (Al_2O_3), were traditionally used to investigate HDO reaction. However, cofeeding with H_2S is required to maintain activity of these catalysts.[47,48] As a result, research attention drifted toward the

Received: September 3, 2019
Revised: October 26, 2019
Published: November 1, 2019

Downloaded via UNIV OF BIRMINGHAM on November 21, 2019 at 14:01:49 (UTC).
See https://pubs.acs.org/sharingguidelines for options on how to legitimately share published articles.

© 2019 American Chemical Society

DOI: 10.1021/acs.energyfuels.9b02993
Energy Fuels 2019, 33, 11712−11723

use of noble metals, which includes ruthenium (Ru), platinum (Pt), palladium (Pd), and rhodium (Rh) as HDO catalysts.[49,50] These catalysts are active at moderate operating conditions and do not require sulfur addition to remain active. However, the ease with which they are poisoned and the availability of these metals pose economic concern.[51,52] Transition metal carbides, nitrides, oxides, and phosphides recently gained attention as low-cost and readily available alternative catalysts for HDO reaction. For instance, Shit et al.[53] reported the use of cobalt phosphides on porous organic polymers (POPs) as catalyst for vanillin HDO reaction. However, concerns on the stability of these catalysts under typical conditions for HDO limit their application. Remarkably, the majority of the previous works on kinetics of vanillin HDO reaction utilized monometallic catalysts such as Ru/C by Bindwal and Vaidya[54] and Pt/C by Sulman et al.[55] However, as previously highlighted, these catalysts are prone to poisoning. Fortunately, their resistance against poisoning can be improved when combined with another metal. In addition, bimetallic catalysts have demonstrated superior HDO performances in terms of selectivity toward deoxygenated products and conversion in past works.[56]

Nonetheless, information on the reaction kinetics of vanillin over bimetallic catalysts is still missing in the literature. In this work a bimetallic catalyst comprising palladium and rhodium on alumina support ($PdRh/Al_2O_3$) was synthesized, characterized, and used to investigate the kinetics of vanillin HDO reaction in the liquid phase. The interaction between Pd and Rh is expected to improve the selectivity toward creosol, a potential future fuel product. Remarkably, the reaction kinetics of vanillin HDO in the presence of other major lignin-derived compounds has not been reported anywhere. The aim of this work is to fill the identified gap in kinetic studies of HDO reaction. On the basis that competition for finite catalyst active sites increases with the addition of another model compound, the energy barrier to vanillin HDO reaction will most likely be higher in the presence of acetic acid. To test these assumptions, the effects of reaction temperature, catalyst loading, hydrogen gas pressure, and initial VL concentration were studied under a kinetically controlled regime in vanillin–acetic acid mixture and vanillin-only environments.

2. EXPERIMENTAL SECTION

2.1. Materials and Catalyst Preparation. Vanillin (purity 99%), vanillyl alcohol (4-hydroxy-3-methoxybenzyl alcohol, purity 99%), creosol (2-methoxy-4-methylphenol, purity 99%), ethyl acetate (purity 99%), and $PdCl_2$ solution (5 wt % in 10 wt % HCl) were purchased from Sigma-Aldrich, United Kingdom. Methanol (purity 99.9%) was obtained from Alfa Aesar, United Kingdom. Hydrogen (H_2) and nitrogen (N_2) gas cylinders (purity 99.9%) were supplied by BOC, United Kingdom. Commercial 5 wt % Rh/Al_2O_3 catalyst was purchased from Johnson–Matthey PLC Catalyst, United Kingdom. The catalyst used to conduct this study was prepared via wet incipient impregnation method. This method involves the addition of 10.0 g of $PdCl_2$ solution dropwise to a slurry containing 10.0 g of Rh/Al_2O_3 and 30 mL of methanol under slow stirring to achieve the desired Pd loading of 2.7 wt %. The solution was stirred at room temperature for an additional 4 h. Subsequently, the resultant mixture was filtered, washed, and dried in a fume cupboard overnight. Further drying in an oven set at 353 K was carried out for 2 h prior to calcination at 773 K for 4 h.

2.2. Catalyst Characterization. The characteristic length and apparent density of the catalyst were obtained from Micrometrics Autopore IV 9500 mercury porosimeter using low- (0–345 kPa) and high-pressure (up to 228 MPa) analysis. Crystallinity of fresh catalysts were examined by XRD using a Bruker AXS GmbH (D8 Advanced XRD, Karlsruhe, Germany). An HITACHI TM3030 Plus Tabletop Scanning Electron Microscope (SEM) equipped with Energy Dispersive X-ray (EDX) analyzer was used to examine the surface morphology of the catalyst before and after the reaction. The characteristics of surface metallic atoms such as active particle diameter and dispersion were determined through CO chemisorption using a Quantachrome ChemBet Pulsar instrument. In addition, the Brunauer–Emmett–Teller (BET) specific surface area, micropore volume, and average pore diameter of the fresh catalyst were determined according to ASTM C1274 using Micromeritics Analytical Instrument ASAP 2010.

2.3. Reactor System and Procedure. The experimental setup and schematic of reactor system used in this work has been described comprehensively by Aliu et al.[57] In a typical experiment, the autoclave was loaded with the appropriate amount of vanillin (2.2–4.4 g), $PdRh/Al_2O_3$ catalyst (0.10–0.25 g), acetic acid (3.85–7.70 g), and 48.6 g of ethyl acetate as solvent. To create an inert atmosphere for impending reaction, the autoclave was purged with N_2 gas. After the purging process, the autoclave was heated to the desired reaction temperature (308–328 K). Once the autoclave attained the desired reaction temperature, the stirring speed was increased to 1000 rpm and H_2 gas was introduced until the desired reaction pressure (1.0–4.0 MPa) was achieved. Timing of the reaction commenced from the point at which H_2 gas was charged. Further details of the experimental procedure were reported by Aliu et al.[57]

2.4. Product Analysis. Reaction samples were initially analyzed via a gas chromatography unit equipped with mass spectrometer (GC-MS) to establish the products formed. Subsequently, multipoint calibration curves were developed to quantify the products and reactants. An automated trace gas chromatography unit equipped with flame ionization detector (GC-FID) containing a mild polar capillary column (i.e., ZB wax with specification of 250 μm internal diameter, 0.25 μm film thickness, and 30 m column length) was deemed suitable for the quantification process. Details on the temperature program applied are reported elsewhere.[57]

3. THEORETICAL BASIS

3.1. Mass and Heat Transfer Effect. The collection of reliable quantitative kinetic data requires the absence of external and internal transport limitations; this includes heat and mass transfer effects.[58] In a typical heterogeneous catalytic reaction such as VL HDO, the following events occur: (i) diffusion of VL and H_2 through the boundary layer surrounding the catalyst particle; (ii) intraparticle diffusion of VL and H_2 into the catalyst pores to the active sites; (iii) adsorption of VL and H_2 onto active sites of the catalyst; (iv) surface reactions to convert adsorbed VL and H_2 into intermediates and possibly surface diffusion steps; (v) desorption of products (i.e., vanillyl alcohol and creosol) from active sites of the catalyst; (vi) intraparticle diffusion of vanillyl alcohol and creosol through pores of the catalyst; (vii) diffusion of vanillyl alcohol and creosol across the boundary surrounding the catalyst.[57] However, the scope of the present work necessitates consideration of only conditions within the intrinsic reaction kinetics control regime (i.e., steps 3–5). Transport limitations as a result of thermal gradients are insignificant at low temperatures.[59] Hence, it was decided to study only the temperature range of 308–328 K. The conventional approaches used to eliminate mass transfer limitations involve agitation speed and catalyst particle size tests to respectively determine the minimum stirring speed and the maximum particle size at which external and internal resistances become insignificant. These tests were performed at a reaction temperature of 318 K. In addition to these tests, the Weisz–Prater criterion was used to verify the absence of

DOI: 10.1021/acs.energyfuels.9b02993
Energy Fuels 2019, 33, 11712–11723

internal diffusion limitations. According to the Weisz−Prater criterion, the absence of significant internal diffusion is confirmed if the dimensionless parameter known as observable modulus ($\eta\varphi^2$) has a value of <0.3 for reaction orders ≤2.[60] From the definition of observable modulus ($\eta\varphi^2$) in eq 1, values significantly <1 indicate faster internal mass transfer rate compared to reaction rate.[61]

$$\eta\phi^2 = \frac{r_0 \omega L^2}{C_i D_{e_i}}, \text{ where } i = \text{VL, } H_2 \quad (1)$$

Herein, r_0 represents the initial reaction rate, η is the effectiveness factor, φ it the Thiele modulus, ω is the catalyst loading, and L is the characteristic length of the spherical catalyst particle. The correlation suggested by Pintar et al.[62] was used to estimate C_H (kmol/m^3), while the Wilke−Chang equation[63] was used to estimate the liquid-phase effective diffusivities of VL and H_2. The initial reaction rate representative of activity was estimated from the conversion−time data using the procedure described by Chen et al.[64] Following a review of the literature[58,60] on mass and heat transfer verification in laboratory-scale reactors, the Madon−Boudart test is the most definitive approach for establishing transport limitation significance. According to this test, in the kinetically controlled regime, the catalyst activity is directly proportional to the number of active sites. Hence, the In−In plot of the catalyst activity against surface metal atom concentration should be linear with a slope of unity to confirm absence of transport limitation.[60] This test was carried out at 318 and 328 K to confirm the absence of both mass and heat transfer resistances in the system.

4. RESULTS AND DISCUSSION

4.1. Catalyst Characterization. The physicochemical properties of synthesized $PdRh/Al_2O_3$ catalyst are shown in Table 1. All the catalysts exhibit mesoporous and type IV isotherm characteristics. Notably, post impregnation of the Pd metal into Rh/Al_2O_3 catalyst, the specific surface area decreased from 164 to 145.5 m^2/g. On the basis of the CO chemisorption analysis, 12% of the metals in the prepared bimetallic $PdRh/Al_2O_3$ catalyst are exposed on the catalyst surface as well as accessible to the reactants.

Table 1. Physicochemical Properties of Fresh $PdRh/Al_2O_3$ Catalyst

property	$PdRh/Al_2O_3$	Rh/Al_2O_3	Pd/Al_2O_3
characteristic length[a] (μm)	13.8	13.6	26.3
average pore diameter[b] (nm)	7.67	7.5	5.0
BET surface area[b] (m^2/g)	145.5	164	108
metal dispersion[c] (%)	12.1		
micropore vol[b] (cm^3/g)	0.27	0.31	0.13
apparent density[a] (g/mL)	4.9	4.7	3.4
Rh[d] (wt %)	3.8	5.0	
Pd[d] (wt %)	2.7		5.0

[a]Determined from mercury porosimetry. [b]Determined from N_2 adsorption−desorption isotherms at 77.5 K. [c]Determined from CO chemisorption. [d]Determined from X-ray fluorescence (XRF) analysis.

Figure 1 shows the scanning electron microscopy with energy-dispersive X-ray spectroscopy (SEM-EDX) of the monometallic Rh/Al_2O_3 and the prepared bimetallic $PdRh/Al_2O_3$ catalysts. The EDX images in parts b and f of Figure 1 confirmed the monometallic and bimetallic catalyst compositions, respectively. It can be seen from Figure 1h that Pd metals are well-dispersed in the prepared bimetallic $PdRh/Al_2O_3$ catalyst.

XRD is a common analytical technique used to identify phases and crystallinity of a sample material such as the prepared $PdRh/Al_2O_3$ catalyst. The XRD patterns of the commercial monometallic Pd/Al_2O_3, unmodified commercial Rh/Al_2O_3, and Pd-modified Rh/Al_2O_3 catalyst to produce bimetallic $PdRh/Al_2O_3$ catalyst are shown in Figure 2. The prominent peaks positioned at 2θ = 10.5°, 45.7°, and 67° can be ascribed to alumina, while the expected positional peaks of Pd metals in the region 31°−40.4° overlapped with alumina. The expected peaks of Rh (311) at 2θ = 86 are not prominent in both the unmodified Rh/Al_2O_3 and synthesized $PdRh/Al_2O_3$. This suggests poor crystallinity of Rh metals in the unmodified Rh/Al_2O_3 and prepared $PdRh/Al_2O_3$ because the intensity of peaks on the XRD pattern normally represents the extent of crystallinity. According to the XRF analysis carried out, the synthesized $PdRh/Al_2O_3$ catalyst contains 2.7% Pd and 3.8% Rh. The crystallite sizes of the metals on the alumina support obtained from the Scherrer equation are as follows: 6.4 nm (Pd/Al_2O_3), 5.9 nm (Rh/Al_2O_3), and 6.1 nm ($PdRh/Al_2O_3$) using peaks at 2θ = 45° and 67°.

The SEM images and particle size distribution of $PdRh/Al_2O_3$ catalyst before and after reaction presented in Figure 3 show no significant difference in packing of the particles. In addition, the energy dispersive x-ray (EDX) analysis showed no carbon deposition on the used catalyst surface (Figure 3a and c). This thereby indicates that the reaction did not induce any observable change in the structure of the catalyst particles. This observation is in agreement with reports in the literature that catalyst deactivation as a result of carbon deposition is less likely at mild operating temperatures.[57,65,66] However, the particle size distribution before and after reaction (Figures 3b and d) shows that 95% of the fresh catalyst particles have sizes within the range of 200−400 nm. Likewise the sizes of 93% of reused catalyst particles fall within the interval of 200−400 nm. Therefore, this indicates a slight drop in the proportion of catalyst particle sizes within the range of 200 nm and an increase in particle size of 300 nm. This may be as a result of little agglomeration of the particles of 200 nm into 300 nm.

4.2. Verification of Kinetically Controlled Reaction Regime. To establish the influence of external and internal transfer limitations, the effect of agitation speed and particle size on initial reaction rates (r_o) was examined. Figure 4a depicts the effect of agitation speed, and Figure 4b represents the influence of particle size. Interestingly, Figure 4a shows that the initial reaction rate is independent of stirring speed in the range of 900−1300 rpm. Therefore, external diffusion limitation is absent when the stirring speed falls within this range. All further experiments in this work were carried out at a stirring speed of 1000 rpm. Figure 4b shows that intraparticle diffusion limitation is negligible for particles smaller than 250 μm. As a result, subsequent experiments were carried out with particles smaller than 250 μm.

To reaffirm the absence of internal mass transfer limitation, eq 1 was used to compute the observable modulus at 318 K. The results are presented in Table 2; because the computed observable moduli for both VL and H_2 were significantly <1, it can be concluded that internal mass transfer resistance is negligible. In addition, the observable modulus of H_2 found is 10 times bigger than that of VL, therefore confirming H_2 as the

DOI: 10.1021/acs.energyfuels.9b02993
Energy Fuels 2019, 33, 11712−11723

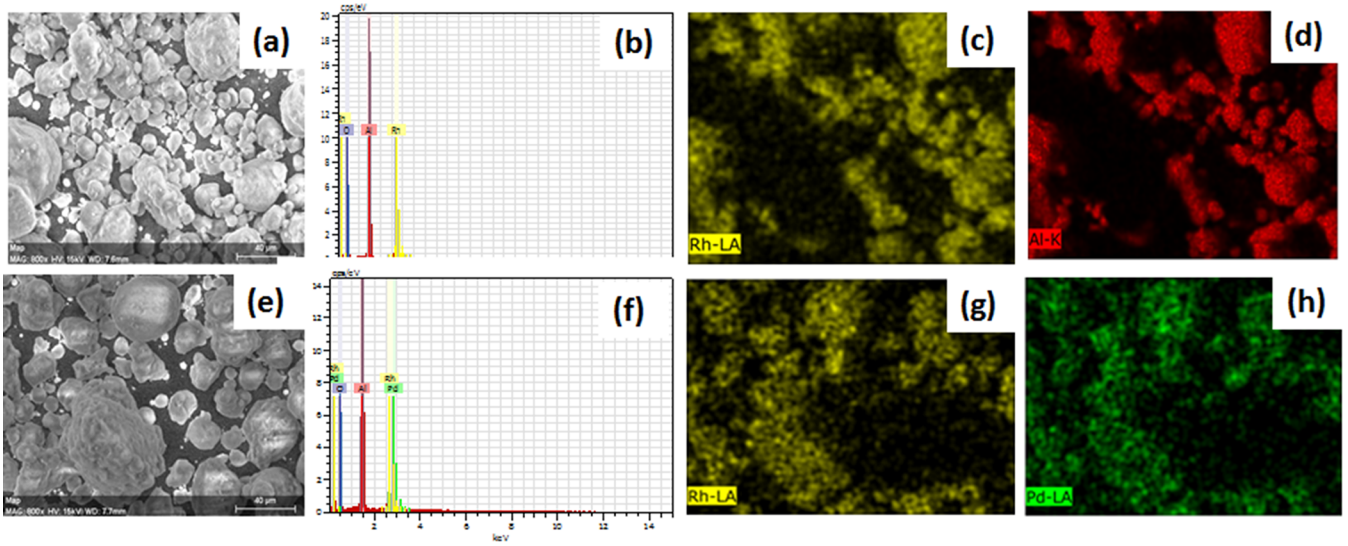

Figure 1. SEM-EDX of Rh/Al_2O_3 (a–d) and prepared $PdRh/Al_2O_3$ (e–h). (a) SEM micrograph of Rh/Al_2O_3 catalyst, (b) EDX of Rh/Al_2O_3 catalyst, (c) mapping of Rh in monometallic catalyst, (d) mapping of Al_2O_3 in monometallic catalyst, (e) SEM micrograph of $PdRh/Al_2O_3$ catalyst, (f) EDX of $PdRh/Al_2O_3$ catalyst, (g) mapping of Rh in the bimetallic catalyst, and (h) mapping of Pd in the bimetallic catalyst.

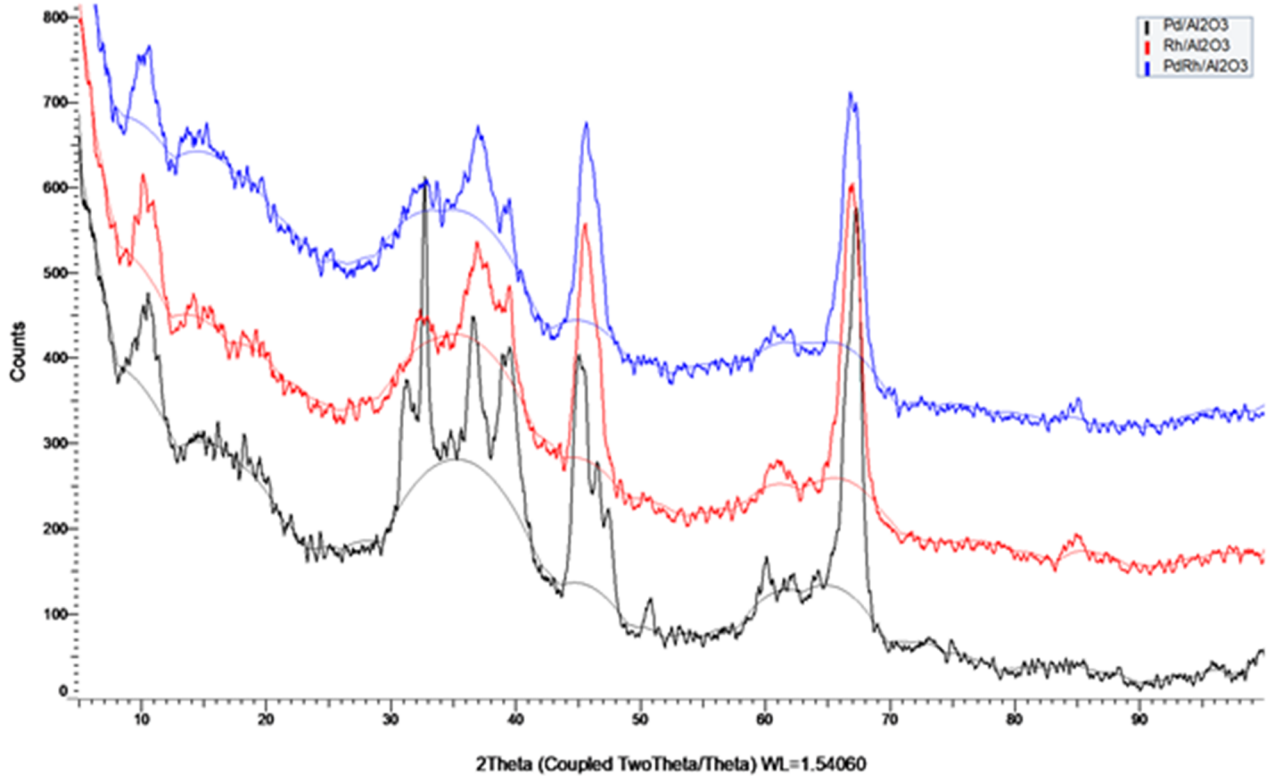

Figure 2. XRD patterns of Pd/Al_2O_3, Rh/Al_2O_3, and prepared $PdRh/Al_2O_3$ catalysts.

limiting reactant within the system. The obtained observable modulus values also indicate that the order of reaction with respect to H_2 gas partial pressure and VL concentration is ≤ 2.

4.3. Preliminary Experiments. The role of Pd, Rh, and Al_2O_3 support on the reaction was examined by conducting experiments with no catalyst, Al_2O_3 support (0.25 g), 5% Rh/Al_2O_3 (0.25 g), 5% Pd/Al_2O_3 (0.25 g), and the prepared $PdRh/Al_2O_3$ catalyst (0.25 g) using 263 mM initial vanillin (VL) solution at 2.0 MPa hydrogen gas partial pressure, 1000 rpm agitation speed, and temperature of 318 K. The results from these experiments are summarized in Table 3. It shows an appreciable amount of products and conversion less than 4% in the absence of a catalyst, while selectivity to creosol increased from 34.8% to 43.7% following addition of the alumina support. However, the change in VL conversion following addition of the alumina support is insignificant. Conversely, in the presence of either Rh/Al_2O_3 or Pd/Al_2O_3, VL conversion increased by approximately 20% (with Rh/Al_2O_3) and 94% (with Pd/Al_2O_3) relative to alumina only. Interestingly, only 4.3% selectivity toward the desired deoxygenated product creosol (CR) was achieved using Pd/Al_2O_3, while in the presence of Rh/Al_2O_3 selectivity toward creosol increased to

DOI: 10.1021/acs.energyfuels.9b02993
Energy Fuels 2019, 33, 11712–11723

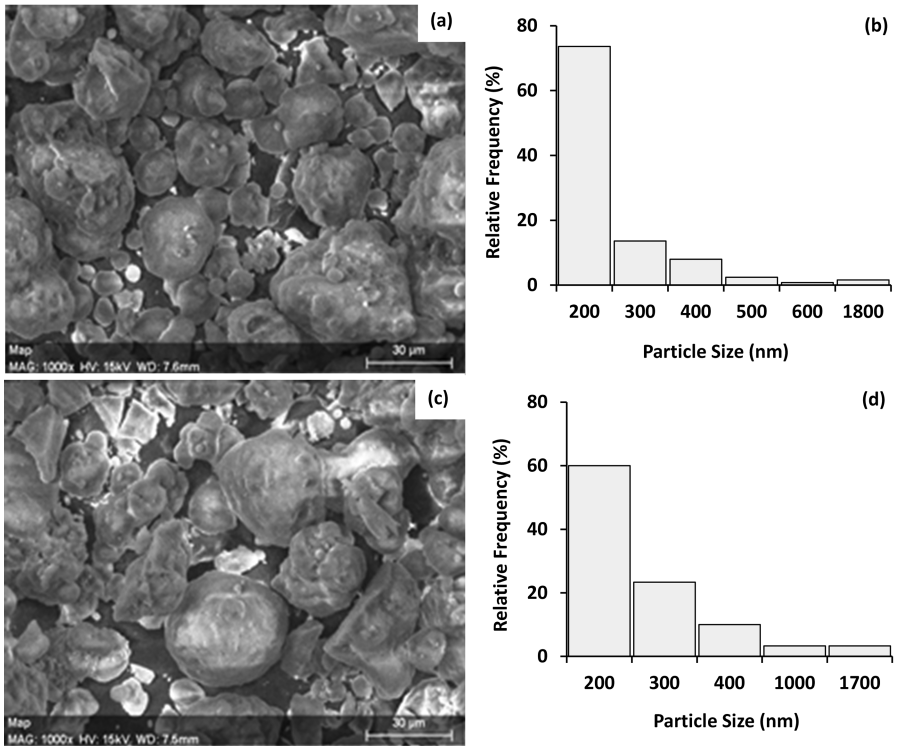

Figure 3. SEM images and the particle size distribution of the fresh (a, b) and spent (c, d) $PdRh/Al_2O_3$ catalyst.

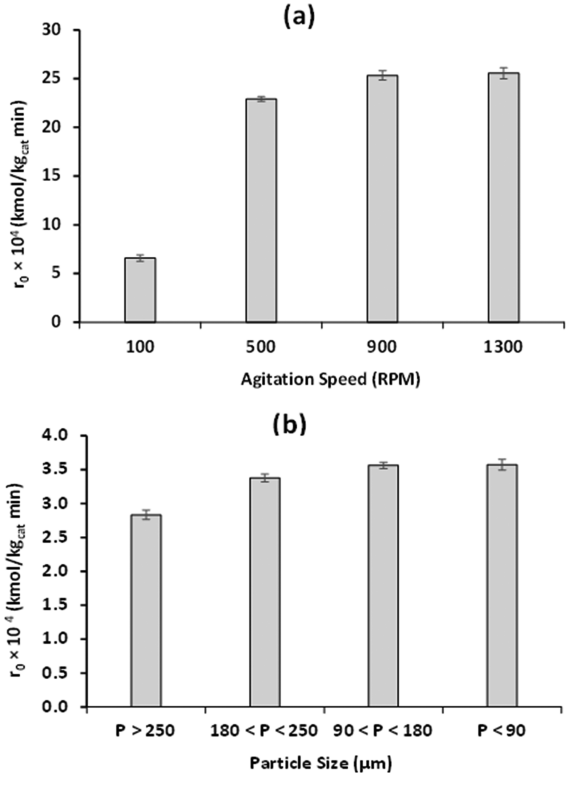

Figure 4. Dependence of the initial reaction rates on (a) agitation speed and (b) particle size.

49.9%. On the basis of this result, Pd/Al_2O_3 favors the conversion of VL to the intermediate product vanillyl alcohol (VA) and Rh/Al_2O_3 favors deoxygenation of VA to CR. This observation stimulated the use of bimetallic catalyst comprising palladium and rhodium on alumina support in this work.

Table 2. Results of Weisz–Prater Analysis at 318 K

parameter	values	
ω (kg/m^3)	1.9	4.6
C_{VL0} (mM)	263.0	263.0
C_{H2} (mM)	2.7	2.7
$r \times 10^3$ (kmol/(kg catalyst min))	1.68	1.56
L (m)	13.8×10^{-6}	13.8×10^{-6}
$D_{e,VL} \times 10^9$(m^2/s)	2.01	2.01
$D_{e,H2} \times 10^8$(m^2/s)	1.77	1.77
$\eta\varphi_{vl}^2$	1.88×10^{-5}	4.4×10^{-5}
$\eta\varphi_H^2$	2.08×10^{-4}	4.8×10^{-4}

Table 3. Results of Preliminary Investigation using Al_2O_3, Rh/Al_2O_3, Pd/Al_2O_3, and $PdRh/Al_2O_3$

experiments	C_{VL} (mM)	C_{VA} (mM)	C_{CR} (mM)	X (%)
no catalyst	253	44.9	24.0	3.88
alumina (Al_2O_3)	250	39.4	30.6	5.13
Rh/Al_2O_3	196	37.9	37.7	25.4
Pd/Al_2O_3	2.63	249	11.2	99.0
$PdRh/Al_2O_3$	0.7	1.4	279	99.7

Clearly, the result in Table 3 provides further justification for the suitability of $PdRh/Al_2O_3$ for VL HDO reaction as it shows significantly improved selectivity toward CR (99.5%) and high conversion (99.7%).

In this study, the typical concentration–time profile observed is presented in Figure 5. It clearly confirmed VA as the intermediate product and CR as the final product, thereby supporting the proposed mechanism in the literature for VL HDO reaction.[54,55,57]

4.4. Effect of Catalyst Loading. The influence of catalyst loading (ω) on the initial rates of VL disappearance (r_0) was studied over the range of 1.86–4.64 kg/m^3 at T = 318 and 328

DOI: 10.1021/acs.energyfuels.9b02993
Energy Fuels 2019, 33, 11712–11723

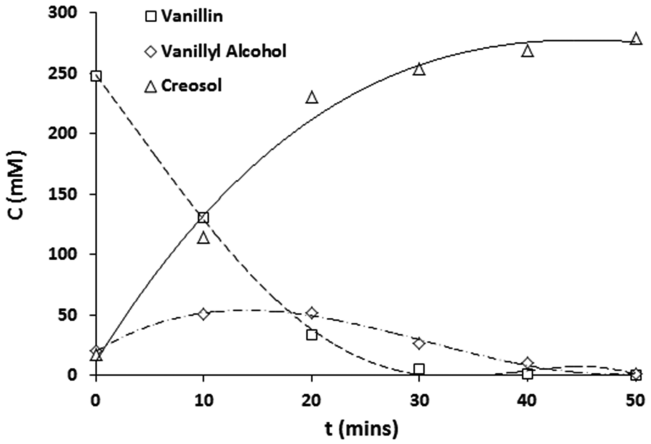

Figure 5. Typical concentration against time profile at 1000 rpm, T = 318 K, P_H = 2.0 MPa, C_{VL0} = 263 mM, and ω = 4.64 kg/m^3. Lines represent best polynomial fit to the data.

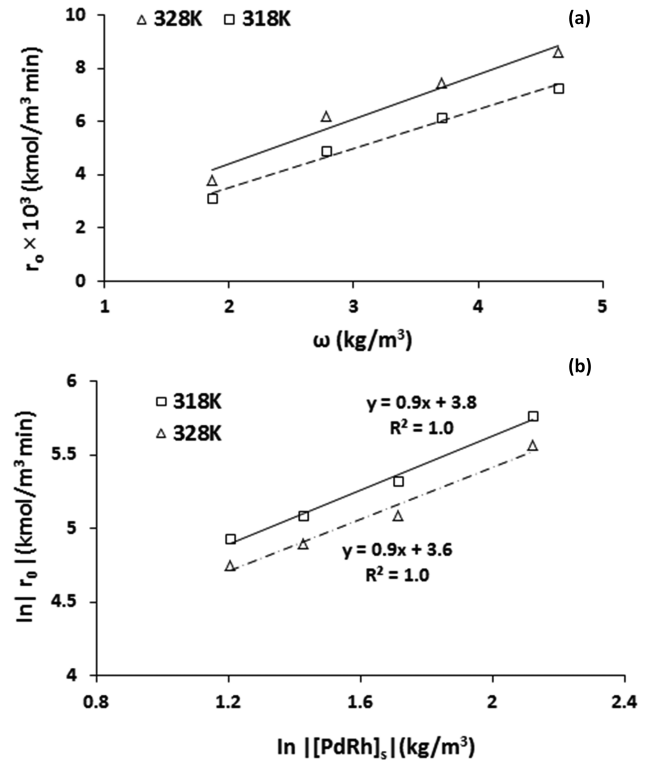

Figure 6. (a) Effect of catalyst loading on initial rate of VL HDO reaction and (b) In−In plot of catalyst activity against surface metal concentration Madon−Boudart test for VL HDO reaction. Lines represent best linear fit to the data.

K, P_H = 3.0 MPa, and initial VL concentration (C_{VL0}) = 263.0 mM. Figure 6a summarizes observed change in r_0 as ω increases, while Figure 6b depicts In−In plot of the catalyst activity against surface metal atom concentration. Notably at 318 and 328 K, Figure 6a showed that r_0 increases as ω increases at both temperatures, thereby suggesting that, under the conditions examined, VL HDO reaction rate is dependent only on the number of active sites. This only holds in the kinetically controlled regime as previously explained in section 3. Indeed, this is the case, because a slope of 0.9 was obtained from the In−In plots in Figure 6b at two different reaction temperatures. On this basis, it can be concluded that both mass

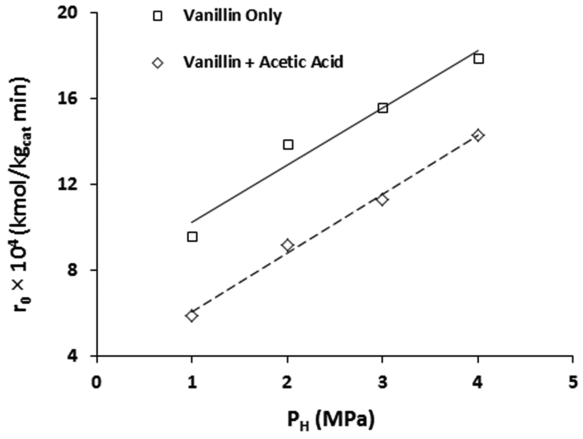

Figure 7. Comparison of the changes in predicted and experimental concentrations of VL in (a) nonacidic and (b) acidic environments at 308, 318, and 328 K. Lines represent fit of model to experimental data.

Table 4. Effect of Initial VL Concentration (C_{VL0}) on Initial VL Disappearance Rates (r_0)

feed solution composition		
C_{VL} (mM)	C_{AA} (mM)	$r_0 \times 10^4$ (kmol/kg$_{cat}$ min)
263	0	13.9
351	0	11.1
438	0	9.1
526	0	7.6
263	1166	9.2
351	1559	7.9
438	1944	6.4
526	2331	4.2

Table 5. Effect of Changes in Starting VL Concentration on Product Selectivity

feed composition		selectivity (%)	
C_{VL} (mM)	C_{AA} (mM)	VA	CR
263	0	0.5	99.5
351	0	38.4	61.6
438	0	60.2	39.8
526	0	68.9	31.1
263	1166	17.7	82.3
351	1559	28.4	71.6
438	1944	45.3	54.7
526	2331	61.0	39.0

and heat transfer resistances are absent (see section 3), thereby reaffirming the conclusion of no transport limitation in the system in section 4.2. The initial turnover frequency (TOF) values corresponding to the r_0 shown in Figure 6a are in the range of 21.1−22.7 min^{-1} at 318 K and 25.2−27.9 min^{-1} at 328 K. In comparison to previous works on monometallic Pd/C and Ru/C catalysts, these values are higher and thus confirm superior activity of the synthesized PdRh/Al_2O_3 catalyst.[54,57]

4.5. Effect of H_2 Gas Partial Pressure. The effect of hydrogen gas partial pressures (P_H) on initial rates of VL disappearance (r_0) was investigated in vanillin−acetic acid and vanillin-only environments at 318 K. Figure 7 represents observed variation in r_0 as P_H changes from 1.0 to 4.0 MPa. It shows that, in vanillin-only environment, r_0 increased from 9.6 × 10^{-4} to 17.9 × 10^{-4} kmol/kg$_{cat}$ min as P_H increases from

DOI: 10.1021/acs.energyfuels.9b02993
Energy Fuels 2019, 33, 11712−11723

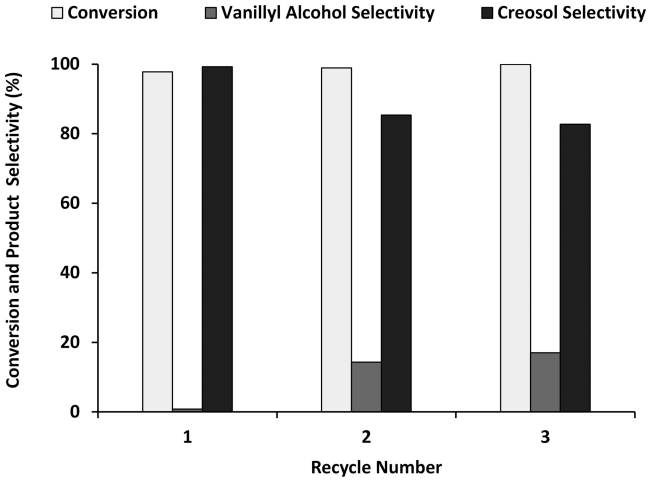

Figure 8. Catalyst stability and reusability test for VL HDO reaction with ethyl acetate as solvent over $PdRh/Al_2O_3$ catalyst. Conditions: T = 338 K; ω = 4.64 kg/m^3; 1000 rpm; 2.0 MPa; C_{VL0} = 263 mM; and t = 1 h.

1.0 to 4.0 MPa. Likewise in the vanillin−acetic acid mixture, r_0 increased from 2.7 × 10^{-4} to 6.6 × 10^{-4} kmol/kg$_{cat}$ min following changes in P_H from 1.0 to 4.0 MPa. Hence, an increase in H_2 gas partial pressure enhances VL HDO reaction in both vanillin−acetic acid and vanillin-only environments. This conclusion complements the initial finding in section 4.2 that H_2 gas is the limiting reactant in the system. The order of reaction with respect to P_H found from the slope of In (r_0) against In (P_H) in Figure S1 is 0.44 in the vanillin-only environment and 0.63 in vanillin−acetic acid mixture. On the basis of the obtained values, it can be concluded that VL HDO reaction exhibits nonfirst-order reaction kinetics with respect to hydrogen gas partial pressure in vanillin-only and vanillin−acetic acid environments. Again, this is in agreement with the earlier claim in section 4.2 that the reaction order with respect to (wrt) P_H is <2. Interestingly, the nonfirst-order dependence on P_H reported in this study is in agreement with previous work on VL HDO reaction over monometallic Pd/C catalyst.[57] Notably, a similar observation of nonfirst-order dependence on P_H was reported in the work of Wan et al.[67] on hydrogenation of 2-butanone over Ru/C catalyst using water as the reaction solvent.

4.6. Effect of Initial VL Concentration. The effect of starting VL concentration (C_{VL0}) on the initial rate of disappearance (r_0) was investigated at 318 K in vanillin-only and vanillin−acetic acid environments, with the values of P_H and ω kept at 2.0 MPa and 4.64 kg/m^3, respectively. The results are summarized in Table 4; it shows that r_0 decreased from 13.9 × 10^{-4} to 7.6 × 10^{-4} kmol/kg$_{cat}$ min as C_{VL0} increased from 263 to 526 mM in the vanillin-only environment. Similarly, in the vanillin−acetic acid environment, r_0 decreased from 9.2 × 10^{-4} to 4.2 × 10^{-4} kmol/kg$_{cat}$ min as C_{VL0} increased from 263 to 526 mM. The observed trend is unusual but in agreement with findings from Aliu et al.[57] on VL hydrodeoxygenation over Pd/C catalyst. Interestingly, the work of Maccarrone et al.[68] on hydrogenation of 1-heptyne over alumina-supported Pd and Ni showed the same trend of initial reaction rates decreasing as starting concentration increases. This unusual trend suggests decreased catalytic activity as C_{VL0} increases, possibly because of increased competition for a finite number of active sites. In addition, it indicates nonfirst-order dependence on VL concentration. In fact, from the plot of In (r_0) against In (C_{VL0}) in Figure S2, the order of reaction wrt VL concentration found is −0.8 (in vanillin-only environment) and −1.1 (in vanillin−acetic acid environment). These values reaffirm the conclusion in section 4.2 regarding the reaction order with respect to VL from the estimated VL observable modulus. In comparison to the value of −0.7 reported as the order of reaction wrt VL concentration in the work of Aliu et al.,[57] the values found in this study are in the same range. Hence, the change in catalyst from monometallic Pd/C to $PdRh/Al_2O_3$ had little effect on the reaction dependence on initial VL concentration. Additionally, observed initial rates of VL disappearance were lower in the presence of acetic acid. However, the estimated orders of reaction wrt VL in vanillin−acetic acid and vanillin-only environments are identical.

Table 5 shows the distribution of products in vanillin-only and vanillin−acetic acid environments; the same trend can be observed in the intermediate and final product selectivities as the starting concentration of vanillin increases. Notably the selectivity toward the desired product creosol differs between the vanillin-only and vanillin−acetic acid environments. However, the change cannot be attributed to active site modification. Rather, increased competition for a finite number of sites on the catalyst surface is a more plausible reason for the observed change in reaction rate, activation energy, and product distribution.

Table 6. Derived Rate Expressions for Plausible Kinetic Models

model	rate expression	model description
I	$r = \frac{k_s K_H K_{VL} C_H C_{VL}}{(1 + \sqrt{K_H C_H} + K_{VL} C_{VL})^3}$	vanillin-only environment
II	$r = \frac{k_s K_H K_{VL} C_H C_{VL}}{(1 + K_{VL} C_{VL} + K_A C_A + \sqrt{K_H C_H})^3}$	vanillin−acetic acid environment

Scheme 1. Vanillin HDO Reaction Steps

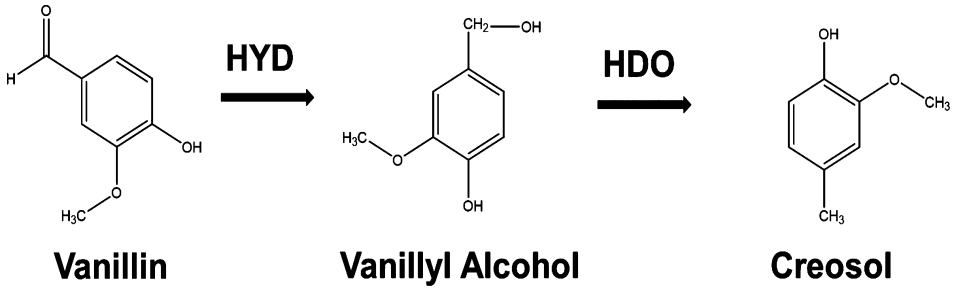

DOI: 10.1021/acs.energyfuels.9b02993
Energy Fuels 2019, 33, 11712−11723

Table 7. Values of Surface Reaction Rate Constants, Adsorption Constants, Heat of Adsorption, and Activation Energy

	vanillin-only environment			vanillin−acetic acid environment		
parameter	308 K	318 K	328 K	308 K	318 K	328 K
k_s (kmol/kg_{cat} min)	49.08 ± 2.86	68.03 ± 1.89	87.06 ± 3.28	10.13 ± 0.08	24.03 ± 0.83	33.99 ± 0.16
K_H (m^3/kmol)	0.048 ± 0.006	0.043 ± 0.004	0.0396 ± 0.003	0.20 ± 0.03	0.148 ± 0.005	0.096 ± 0.008
K_{VL} (m^3/kmol)	2.21 ± 0.03	1.99 ± 0.18	1.61 ± 0.05	0.80 ± 0.05	0.70 ± 0.12	0.58 ± 0.03
K_a (m^3/kmol)				0.006 ± 0.0004	0.001 ± 0.0002	0.0005 ± 0.00008
E_A (kJ/mol)		24.1			51.0	
ΔH_H (kJ/mol)		7.8			30.8	
ΔH_{VL} (kJ/mol)		13.4			13.8	
ΔH_A (kJ/mol)					104.8	

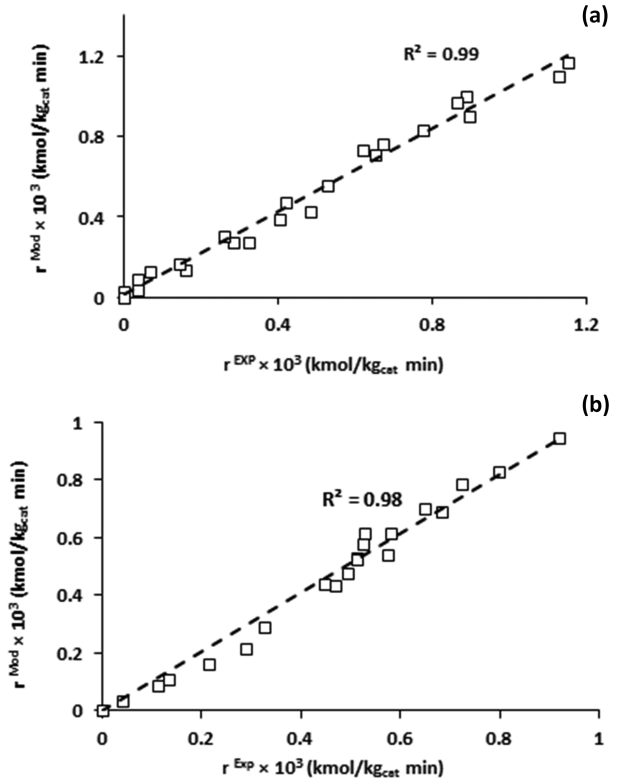

Figure 9. Parity plots comparing predicted and experimental initial reaction rates of VL in (a) nonacidic and (b) acidic environments. Lines represent best fit to data.

4.7. Catalyst Stability and Reusability Test. To examine the stability and reusability of $PdRh/Al_2O_3$ catalyst, it was recycled thrice under the conditions of 338 K, 1000 rpm, 2.0 MPa, and 1 h reaction time using a catalyst loading of 4.67 kg/m^3 and initial VL concentration of 263 mM. Prior to reusing the catalyst, it was dried overnight at room temperature. As shown in Figure 8, conversion, which is indicative of the catalyst activity, remained unchanged throughout the three cycles. However, slight changes can be observed in the product distribution between the first and second cycles. This indicates a small change in metal sites due to the absence of regeneration. Because the rate calculations were based on conversion, which remained the same for the three cycles, it follows that modeling of the reaction kinetics does not require a deactivation term.

4.8. Proposed Scheme for Vanillin HDO. On the basis of the products observed in this study, Scheme 1 represents the proposed steps in vanillin (VL) HDO reaction. Interestingly, this scheme is in agreement with Table 3 in section 4.3 and literature.[54,55,57] The first step involves hydrogenation of VL to vanillyl alcohol (VA), while in the last step VA is further hydrogenated to the product of interest, creosol (CR). At temperatures higher than the range considered in this study, other products like guaiacol and aryl group hydrocarbons may appear as a result of side reactions such as demethylation and decarbonylation.[54,57]

4.9. Modeling of VL HDO Reaction Kinetics. Most of the previous attempts in the literature to model the HDO reaction of VL and other related bio-oil model compounds favored the Langmuir−Hinshelwood−Hougen−Watson (LHHW) approach for reasons elucidated in Aliu et al.[53,57] Hence, the LHHW approach is used in this work to model the reaction kinetics of VL over $PdRh/Al_2O_3$ catalyst. The majority of fluid solid catalytic reactions modeling via the LHHW method assumed that hydrogen adsorbed dissociatively onto the catalyst surface.[69−71] Therefore, the derived rate expressions presented in Table 6 are based on dissociatively chemisorbed hydrogen atoms. The elementary steps associated with competitive adsorption of dissociatively chemisorbed H_2 and VL are represented by eqs 2−4 (see model derivation in section S1).

$$VL + S \leftrightarrow VLS \quad \text{(fast)} \tag{2}$$

$$H_2 + 2S \leftrightarrow 2HS \quad \text{(fast)} \tag{3}$$

$$VLS + 2HS \leftrightarrow P \quad \text{(slow)} \tag{4}$$

In the presence of acetic acid (AA), the elementary steps for competitive adsorption of dissociatively chemisorbed H_2, VL, and AA are represented by eqs 5−8 (see derivation of model for the binary mixture in section S1).

$$VL + S \leftrightarrow VLS \quad \text{(fast)} \tag{5}$$

$$AA + S \leftrightarrow AAS \quad \text{(fast)} \tag{6}$$

$$H_2 + 2S \leftrightarrow 2HS \quad \text{(fast)} \tag{7}$$

$$2HS + VLS \leftrightarrow P \quad \text{(slow)} \tag{8}$$

where H_2 is molecular hydrogen, H is atomic hydrogen, AAS is adsorbed acetic acid intermediate, HS is adsorbed atomic hydrogen, VLS is the adsorbed vanillin intermediate, P is the final product, and S is the catalyst active site. It is worth mentioning that previous work on the VL HDO reaction over Pd/C confirmed the suitability of competitive adsorption models over noncompetitive models,[57] hence the decision in this work to focus only on competitive dissociative adsorption models. In addition, other possibilities of H_2 and VL adsorption steps as the rate-determining step (RDS) have been ruled out in previous work.[57] To estimate the kinetic

DOI: 10.1021/acs.energyfuels.9b02993
Energy Fuels 2019, 33, 11712−11723

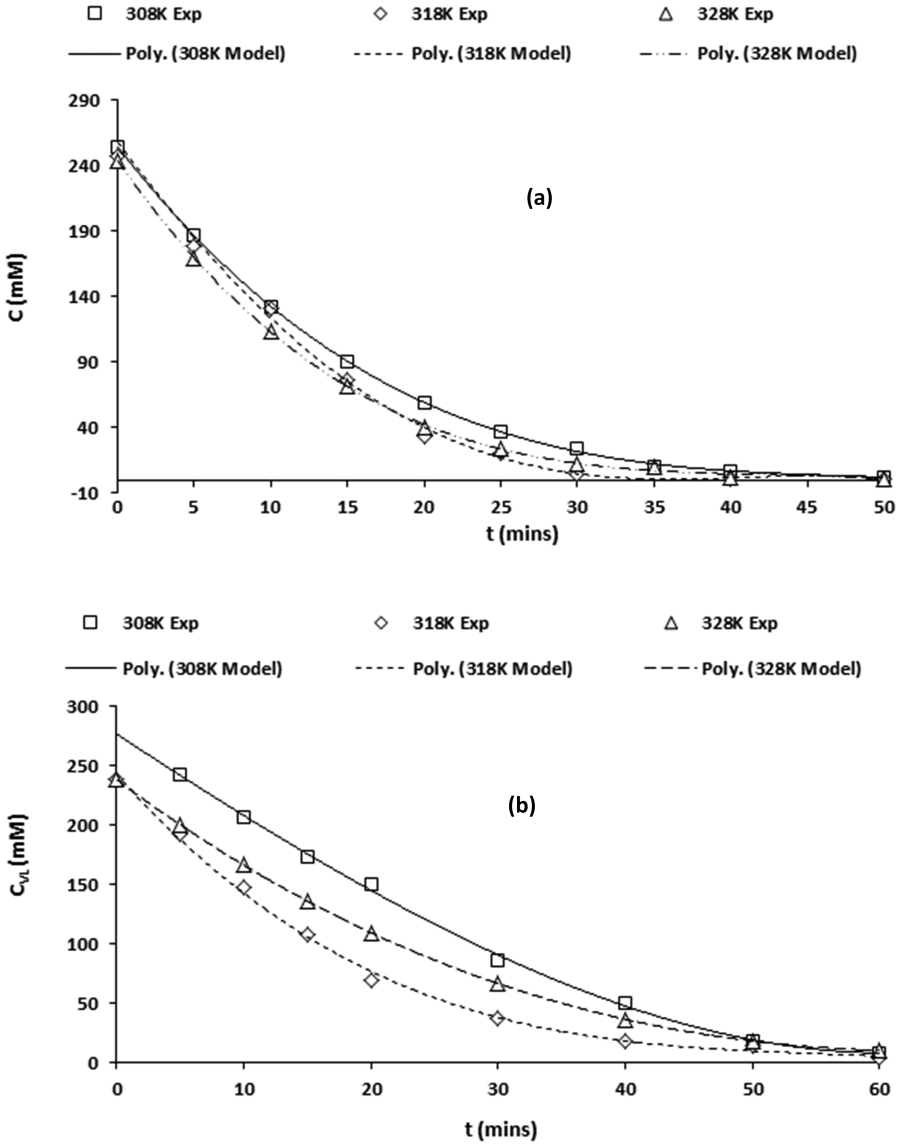

Figure 10. Comparison of the changes in predicted and experimental concentrations of VL in (a) nonacidic and (b) acidic environments at 308, 318, and 328 K. Lines represent fit of model to experimental data.

Table 8. Changes in Fractional Coverage of VL, H_2, Acetic Acid, and Vacant Site over Time at 318 K

	nonacidic medium			acidic environment			
t	θ_V	θ_{VL}	θ_H	θ_V	θ_{VL}	θ_H	θ_A
0	0.665	0.328	0.007	0.844	0.138	0.017	0.001
10	0.787	0.205	0.008	0.891	0.090	0.018	0.001
30	0.980	0.009	0.011	0.955	0.025	0.019	0.001
50	0.988	0.001	0.011	0.970	0.009	0.019	0.001

parameters (i.e., surface reaction rate constant (k_s), hydrogen adsorption constant (K_H), VL adsorption constant (K_{VL}), and acetic acid adsorption constant (K_A) in the rate expressions for vanillin−acetic acid and vanillin-only environments (see Table 6), a nonlinear generalized reduced gradient (GRG) solver in Microsoft Excel was used to minimize the objective function defined as residual sum of squares (RSS) in eq 9.

$$\mathrm{RSS} = \sum (r^{\mathrm{Exp}} - r^{\mathrm{Mod}})^2 \tag{9}$$

Herein, r^{Exp} denotes experimental reaction rates, and r^{Mod} represents predicted reaction rates from the models. The estimated values for surface reaction rate constant, adsorption constants, heat of adsorption, and activation energy are provided in Table 7. These values were estimated using the Arrhenius expression for surface reaction rate constant and Van't Hoff isochore for the heats of adsorption. Interestingly, Table 7 shows that the VL HDO reaction activation energy is ∼2 times higher in the presence of acetic acid. This explains the observed lower initial VL reaction rates in the presence of acetic acid compared to the vanillin-only environment in section 4.6. In comparison to values of 50.6 kJ/mol reported in a previous work by Aliu et al.[57] and 41.2 kJ/mol in the work of Bindwal and Vaidya,[54] the synergy between Pd and Rh metals significantly reduced the VL HDO reaction activation energy; this is consistent with the TOF comparison in section 4.4. However, this benefit diminished when the reaction was carried out in the presence of acetic acid. As shown in Table 7, the estimated activation energy for VL HDO reaction in the presence of acetic acid is the same as the value reported by Aliu

DOI: 10.1021/acs.energyfuels.9b02993
Energy Fuels 2019, 33, 11712−11723

et al.[57] On the basis of the enthalpy of adsorption estimated from the models, it can be concluded that the strengths of adsorptions of both VL and H_2 are significantly smaller compared to that for acetic acid. The strong interaction between the catalyst surface and the acetic acid increased competition for available active sites. As a result, the VL HDO reaction requires higher activation energy in the presence of acetic acid.

The parity plots in parts a and b of Figure 9 illustrate the level of agreement between predicted and observed initial reaction rates of VL in vanillin−acetic acid and vanillin-only environments. Clearly, with R^2 values of 0.99 (vanillin-only environment) and 0.98 (vanillin−acetic acid environment) for the parity plots, the proposed models reliably describe the VL HDO reaction in a batch reactor. Parts a and b of Figure 10 further reaffirm the fit of the proposed models as they indicate strong agreement between predicted and experimental VL concentrations at three different reaction temperatures.

The fractional coverage of H_2, VL, and acetic acid as a function of time can be seen in Table 8. It shows that the fractional coverage of VL decreases over time, while those of H_2 and acetic acid were almost constant. Notably, the mild temperature used in this study accounts for the negligible change in acetic acid coverage. In addition, H_2 coverage did not change over time because of the fixed external H_2 gas supply applied to maintain a constant reaction pressure.

5. CONCLUSIONS

In summary, the specific objective of this work is to examine any differences between the hydrodeoxygenation (HDO) reaction kinetics of vanillin, a typical model compound of bio-oil in pure and acidic environments. In addition, the roles of noble metals such as Pd and Rh on alumina were investigated to obtain a combination of metals that maximizes selectivity toward the desired fuel product creosol. The use of Pd/Al_2O_3 favors the conversion of vanillin (99%) but resulted in low selectivity toward creosol (4%). Conversely, in the presence of Rh/Al_2O_3, low conversion (25%) and high selectivity toward creosol (49%) were achieved. This stimulated the use of $PdRh/Al_2O_3$ to further improve selectivity toward creosol while maintaining high conversion. Interestingly, selectivity toward creosol increased significantly to 99.5% with conversion still hovering above 99% in the presence of $PdRh/Al_2O_3$. Consequently, all other experiments in this work were conducted using the prepared bimetallic $PdRh/Al_2O_3$ catalyst. It was found that stirring speed in the range of 900−1300 rpm and particle size less than 250 μm ensure the absence of transport limitations within the system. In the vanillin-only environment, the order of reaction with respect to VL concentration was −0.8, while with respect to hydrogen gas partial pressure (P_H) the order was 0.44. Conversely, in the presence of acetic acid, the estimated order of reaction with respect to VL concentration was −1.1 and and that with respect to P_H was 0.63. The initial rates of VL disappearance during the reactions in vanillin−acetic acid and vanillin-only environments were modeled through derived rate expressions from the Langmuir−Hinshelwood−Hougen−Watson (LHHW) method. The estimated values from the model for the vanillin-only environment were 24.1 kJ/mol for reaction activation energy, 13.4 kJ/mol for VL adsorption enthalpy, and 7.8 kJ/mol for H_2 adsorption enthalpy. The corresponding values from the modified model for VL HDO reaction in the vanillin−acetic acid environment include 51.0 kJ/mol for the activation energy, 13.8 kJ/mol for VL adsorption enthalpy, and 30.8 kJ/mol for H_2 adsorption enthalpy. On the basis of the results obtained from this study, the presence of acetic acid significantly increased the energy barrier for vanillin HDO reaction.

■ ASSOCIATED CONTENT

Supporting Information

The Supporting Information is available free of charge on the ACS Publications website at DOI: 10.1021/acs.energyfuels.9b02993.

In (r_0) against In (PH) plots; In ($r0$) against In (CVL0) plots; and rate expressions derivation (PDF)

■ AUTHOR INFORMATION

Corresponding Author

*Tel.: +44(0) 121 414 5295. E-mail: j.wood@bham.ac.uk.

ORCID

Abarasi Hart: 0000-0002-4433-5887

Joseph Wood: 0000-0003-2040-5497

Notes

The authors declare no competing financial interest.

Data in this paper are available free of charge via http://edata.bham.ac.uk/.

■ ACKNOWLEDGMENTS

E.A. expresses profound gratitude to School of Chemical Engineering, University of Birmingham, for the financial support provided to complete this research work. In addition, the authors appreciate the support of Dr. Helen Daly and Prof. Christopher Hardacre at the University of Manchester for conducting the CO chemisorption analysis of the catalyst used in this work.

■ ABBREVIATIONS

C_H = concentration of hydrogen in the liquid phase, kmol m^{-3}

C_{VL0} = initial concentration of vanillin in the liquid phase, kmol m^{-3}

CR = creosol

D_{e_i} = effective diffusivity of species i in eq [1], m^2/s

E_A = activation energy of the reaction, kJ/mol

ΔH_H = enthalpy of adsorption for hydrogen, kJ/mol

ΔH_{VL} = enthalpy of adsorption for vanillin, kJ/mol

ΔH_A = enthalpy of adsorption for acetic acid, kJ/mol

HDO = hydrodeoxygenation

K_H = adsorption equilibrium constant for hydrogen gas, m^3/kmol

K_S = surface reaction rate constant, kmol/(kg_{cat} min)

K_{VL} = adsorption equilibrium constant for vanillin, m^3/kmol

K_A = adsorption equilibrium constant for acetic acid, m^3/kmol

L = characteristic length of catalyst particle

LHHW = Langmuir−Hinshelwood−Hougen−Watson

P_H = hydrogen gas partial pressure, MPa

r_o = initial reaction rate, kmol/(kg_{cat} min)

rpm = revolutions per min

r^{Exp} = experimental values of reaction rates, kmol/(kg_{cat} min)

r^{Mod} = reaction rates predicted from LHHW models, kmol/(kg_{cat} min)

DOI: 10.1021/acs.energyfuels.9b02993
Energy Fuels 2019, 33, 11712−11723

R^2 = coefficient of determination
RSS = residual sum of squares
S_i = active site i on the catalyst surface
T = temperature, K
t = time, min
VA = vanillyl alcohol
VL = vanillin
ω = catalyst loading, kg m^{-3}
Φ = Thiele modulus
η = effectiveness factor
$\eta\Phi_i^2$ = observable modulus for species i in eq 1
θ_V = vacant site fractional coverage
θ_{VL} = vanillin fractional coverage
θ_A = acetic acid fractional coverage
θ_H = hydrogen fractional coverage
TOF = turnover frequency, 1/min

REFERENCES

(1) Newell, R.; Raimi, D.; Aidana, G. *Global Energy Outlook 2019: The Next Generation of Energy*; Report 19-06; Resources for the Future: Washington, DC, 2019.
(2) Wang, Y.; He, T.; Liu, K.; Wu, J.; Fang, Y. From biomass to advanced bio-fuel by catalytic pyrolysis /hydro-processing: Hydrodeoxygenation of bio-oil derived from biomass catalytic pyrolysis. *Bioresour. Technol.* **2012**, *108*, 280−284.
(3) Raj, B.; Singh, O. Global Trends of Fossil Fuel Reserves and Climate Change in the 21st Century. *Fossil Fuel and the Environment*; InTech: **2012**; DOI: 10.5772/38655.
(4) Patel, M.; Kumar, A. Production of renewable diesel through the hydroprocessing of lignocellulosic biomass-derived bio-oil: A review. *Renewable Sustainable Energy Rev.* **2016**, *58*, 1293−1307.
(5) Lu, M.; Du, H.; Wei, B.; Zhu, J.; Li, M.; Shan, Y.; Song, C. Catalytic Hydrodeoxygenation of Guaiacol over Palladium Catalyst on Different Titania Supports. *Energy Fuels* **2017**, *31*, 10858−10865.
(6) Lee, H.; Kim, Y. M.; Lee, I. G.; Jeon, J. K.; Jung, S. C.; Chung, J.; Choi, W. G.; Park, Y.-K. Recent advances in the catalytic hydrodeoxygenation of bio-oil. *Korean J. Chem. Eng.* **2016**, *33*, 3299−3315.
(7) Snell, R. *Carbon−Carbon bond forming reactions for bio-oil upgrading: heterogeneous catalyst and model compound studies*, Ph.D. Thesis, Iowa State University, 2012.
(8) Alonso, D. M.; Bond, J. Q.; Dumesic, J. A. Catalytic conversion of biomass to biofuels. *Green Chem.* **2010**, *12*, 1493−1513.
(9) Huber, G. W.; Iborra, S.; Corma, A. Synthesis of Transportation Fuels from Biomass: Chemistry, Catalysts, and Engineering. *Chem. Rev.* **2006**, *106*, 4044−4098.
(10) Huber, G. W.; Corma, A. Synergies between bio- and oil refineries for the production of fuels from biomass. *Angew. Chem., Int. Ed.* **2007**, *46*, 7184−7201.
(11) Chheda, J. N.; Huber, G. W.; Dumesic, J. A. Liquid-phase catalytic processing of biomass-derived oxygenated hydrocarbons to fuels and chemicals. *Angew. Chem., Int. Ed.* **2007**, *46*, 7164−7183.
(12) Serrano-Ruiz, J. C.; Dumesic, J. A. Catalytic routes for the conversion of biomass into liquid hydrocarbon transportation fuels. *Energy Environ. Sci.* **2011**, *4*, 83−99.
(13) Mohan, D.; Pittman, C. U.; Steele, P. H. Pyrolysis of wood/biomass for bio-oil: A critical Review. *Energy Fuels* **2006**, *20*, 848−889.
(14) Dellomonaco, C.; Clomburg, J. M.; Miller, E. N.; Gonzalez, R. Engineered reversal of the oxidation cycle for the synthesis of fuels and chemicals. *Nature* **2011**, *476*, 355−359.
(15) Zhang, X.; Long, J.; Kong, W.; Zhang, Q.; Chen, L.; Wang, T.; Ma, L.; Li, Y. Catalytic upgrading of bio-oil over Ni-based catalysts supported on mixed oxides. *Energy Fuels* **2014**, *28*, 2562−2570.
(16) Bridgwater, A. V. Production of high grade fuels and chemicals from catalytic pyrolysis of biomass. *Catal. Today* **1996**, *29*, 285−295.
(17) Bridgwater, A. V. Catalysis in thermal biomass conversion. *Appl. Catal., A* **1994**, *116*, 5−47.
(18) Boucher, M. E.; Chaala, A.; Pakdel, H.; Roy, C. Bio-oils obtained by vacuum pyrolysis of softwood bark as a liquid fuel for gas turbines. Part II: Stability and ageing of bio-oil and its blends with methanol and a pyrolytic aqueous pahse. *Biomass Bioenergy* **2000**, *19*, 351−361.
(19) Bridgwater, A. V. Review of fast pyrolysis of biomass and product upgrading. *Biomass Bioenergy* **2012**, *38*, 68−94.
(20) Echeandia, S.; Pawelec, B.; Barrio, V. L.; Arias, P. L.; Cambra, J. F.; Loricera, C. V.; Fierro, J. L. G. Enhancement of phenol hydrodeoxygenation over Pd catalysts supported on mixed HY zeolite and Al_2O_3. An approach to O-removal from bio-oils. *Fuel* **2014**, *117*, 1061−1073.
(21) Boullosa-Eiras, S.; Lødeng, R.; Bergem, H.; Stöcker, M.; Hannevold, L.; Blekkan, E. A. Catalytic hydrodeoxygenation (HDO) of phenol over supported molybdenum carbide, nitride, phosphide and oxide catalysts. *Catal. Today* **2014**, *223*, 44−53.
(22) Jae, J.; Tompsett, G. A.; Foster, A. J.; Hammond, K. D.; Auerbach, S. M.; Lobo, R. F.; Huber, G. W. Investigation into the shape selectivity of zeolite catalysts for biomass conversion. *J. Catal.* **2011**, *279*, 257−268.
(23) Li, K.; Wang, R.; Chen, J. Hydrodeoxygenation of anisole over silica-supported Ni2P, MoP, and NiMoP catalysts. *Energy Fuels* **2011**, *25*, 854−863.
(24) Busetto, L.; Fabbri, D.; Mazzoni, R.; Salmi, M.; Torri, C.; Zanotti, V. Application of the Shvo catalyst in homogeneous hydrogenation of bio-oil obtained from pyrolysis of white poplar: New mild upgrading conditions. *Fuel* **2011**, *90*, 1197−1207.
(25) Fisk, C. A.; Morgan, T.; Ji, Y.; Crocker, M.; Crofcheck, C.; Lewis, S. A. Bio-oil upgrading over platinum catalysts using in situ generated hydrogen. *Appl. Catal., A* **2009**, *358*, 150−156.
(26) Diebold, J. P. *A Review of the Chemical and Physical Mechanisms of the Storage Stability of Fast Pyrolysis Bio-Oils*; NREL/SR-570-27613; NREL: 1999; DOI: 10.2172/753818.
(27) Laurent, E.; Delmon, B. applied catalysis A Study of the hydrodeoxygenation of carbonyl, carboxyl. ic and guaiacyl groups over sulfided CoMo/ y-A1203 and NiMo/3/-A1203 catalysts. I. Catalytic reaction schemes. *Appl. Catal., A* **1994**, *109*, 77−96.
(28) Elliott, D. C.; Beckman, D.; Bridgwater, A. V.; Diebold, J. P.; Gevert, S. B.; Solantausta, Y. Developments in Direct Thermochemical Liquefaction of Biomass. *Energy Fuels* **1991**, *5*, 399−410.
(29) Luo, Y.; Guda, V. K.; Hassan, E. B.; Steele, P. H.; Mitchell, B.; Yu, F. Hydrodeoxygenation of oxidized distilled bio-oil for the production of gasoline fuel type. *Energy Convers. Manage.* **2016**, *112*, 319−327.
(30) Pütun, E.; Uzun, B. B.; Putün, A. E. Rapid pyrolysis of olive residue. 2. Effect of catalytic upgrading of pyrolysis vapors in a two-stage fixed-bed reactor. *Energy Fuels* **2009**, *23*, 2248−2258.
(31) Stephanidis, S.; Nitsos, C.; Kalogiannis, K.; Iliopoulou, E. F.; Lappas, A. A.; Triantafyllidis, K. S. Catalytic upgrading of lignocellulosic biomass pyrolysis vapours: Effect of hydrothermal pre-treatment of biomass. *Catal. Today* **2011**, *167*, 37−45.
(32) Choudhary, T. V.; Phillips, C. B. Renewable fuels via catalytic hydrodeoxygenation. *Appl. Catal., A* **2011**, *397*, 1−12.
(33) Elliott, D. C. Historical Developments in Hydroprocessing Bio-oils. *Energy Fuels* **2007**, *21*, 1792−1815.
(34) Furimsky, E. Catalytic hydrodeoxygenation. *Appl. Catal., A* **2000**, *199*, 147−190.
(35) Samolada, M. C.; Baldauf, W.; Vasalos, I. A. Production of a bio-gasoline by upgrading biomass flash pyrolysis liquids via hydrogen processing and catalytic cracking. *Fuel* **1998**, *77*, 1667−75.
(36) Ahmad, M. M.; Nordin, M. R.; Azizan, M. T. Upgrading of Bio-Oil into High-Value Hydrocarbons via Hydrodeoxygenation. *Am. J. Appl. Sci.* **2010**, *7*, 746−755.
(37) Ruddy, D. A.; Schaidle, J. A.; Ferrell, J. R.; Wang, J.; Moens, L.; Hensley, J. E. Recent advances in heterogeneous catalysts for bio-oil upgrading via "ex situ catalytic fast pyrolysis": catalyst development

DOI: 10.1021/acs.energyfuels.9b02993
Energy Fuels 2019, 33, 11712−11723

through the study of model compounds. *Green Chem.* **2014**, *16*, 454−490.
(38) Vispute, T. P.; Huber, G. W. Production of hydrogen, alkanes and polyols by aqueous phase processing of wood-derived pyrolysis oils. *Green Chem.* **2009**, *11*, 1433−1445.
(39) Klass, D. L. Thermal Conversion: Pyrolysis and Liquefaction. *Biomass for Renewable Energy, Fuels, and Chemicals*; Elsevier: 1998; p 651.
(40) Czernik, S.; Bridgwater, A. V. Overview of applications of biomass fast pyrolysis oil. *Energy Fuels* **2004**, *18*, 590−598.
(41) Mu, W.; Ben, H.; Ragauskas, A.; Deng, Y. Lignin Pyrolysis Components and Upgrading-Technology Review. *BioEnergy Res.* **2013**, *6*, 1183−1204.
(42) Hosoya, T.; Kawamoto, H.; Saka, S. Solid/liquid- and vapor-phase interactions between cellulose- and lignin-derived pyrolysis products. *J. Anal. Appl. Pyrolysis* **2009**, *85*, 237−246.
(43) Lou, R.; Wu, S.-b.; Lv, G.-j. Effect of conditions on fast pyrolysis of bamboo lignin. *J. Anal. Appl. Pyrolysis* **2010**, *89*, 191−196.
(44) Lou, R.; Wu, S.-b.; Lv, G.-j.; Guo, D.-l. Pyrolytic products from rice straw and enzymatic/mild acidolysis lignin (EMAL). *BioResources* **2010**, *5*, 2184−2194.
(45) Mullen, C. A.; Boateng, A. A. Catalytic pyrolysis-GC/MS of lignin from several sources. *Fuel Process. Technol.* **2010**, *91*, 1446−1458.
(46) Yang, Q.; Wu, S.; Lou, R.; Lv, G. Analysis of wheat straw lignin by thermogravimetry and pyrolysis-gas chromatography/mass spectrometry. *J. Anal. Appl. Pyrolysis* **2010**, *87*, 65−69.
(47) Gao, D.; Schweitzer, C.; Hwang, H. T.; Varma, A. Conversion of Guaiacol on Noble Metal Catalysts: Reaction Performance and Deactivation Studies. *Ind. Eng. Chem. Res.* **2014**, *53*, 18658−18667.
(48) Senol, O. I.; Viljava, T. R.; Krause, A. O. I. Effect of sulphiding agents on the hydrodeoxygenation pf aliphatic esters on sulphided catalysts. *Appl. Catal., A* **2007**, *326*, 236−244.
(49) Wildschut, J.; Arentz, J.; Rasrendra, C. B.; Venderbosch, R. H.; Heeres, H. J. Catalytic hydrotreatment of fast pyrolysis oil: Model studies on reaction pathways for the carbohydrate fraction. *Environ. Prog. Sustainable Energy* **2009**, *28*, 450−460.
(50) Wildschut, J.; Mahfud, F. H.; Venderbosch, R. H.; Heeres, H. J. Hydrotreatment of fast pyrolysis oil using heterogenous noble-metal catalysts. *Ind. Eng. Chem. Res.* **2009**, *48*, 10324−10334.
(51) Lin, Y. C.; Li, C. L.; Wan, H. P.; Lee, H. T.; Liu, C. F. Catalytic Hydrodeoxygenation of Guaiacol on Rh-Based and Sulfided CoMo and NiMo catalysts. *Energy Fuels* **2011**, *25*, 890−896.
(52) Elliott, D. C.; Hart, T. R. Catalytic Hydroprocessing of Chemical Models for Bio-oil. *Energy Fuels* **2009**, *23*, 631−637.
(53) Shit, S. C.; Koley, P.; Joseph, B.; Marini, C.; Nakka, L.; Tardio, J.; Mondal, J. Porous Organic Polymer-Driven Evolution of High Performance Cobalt Phosphide Hybrid Nanosheets as Vanillin Hydrodeoxygenation Catalyst. *ACS Appl. Mater. Interfaces* **2019**, *11*, 24140−24153.
(54) Bindwal, A. B.; Vaidya, P. D. Reaction kinetics of vanillin hydrogenation in aqueous solutions using a Ru/C catalyst. *Energy Fuels* **2014**, *28*, 3357−3362.
(55) Sulman, A.; Mäki-Arvela, P.; Bomont, L.; Fedorov, V.; Alda-Onggar, M.; Smeds, A.; Hemming, J.; Russo, V.; Warna, J.; Kaldstrom, M.; Murzin, D. Y. Vanillin Hydrodeoxygenation: Kinetic Modelling and Solvent Effect. *Catal. Lett.* **2018**, *148*, 2856−2868.
(56) Elliott, D. C. Biofuel from fast pyrolysis and catalytic hydrodeoxygenation. *Curr. Opin. Chem. Eng.* **2015**, *9*, 59−65.
(57) Aliu, E.; Hart, A.; Wood, J. Kinetics of Vanillin Hydrodeoxygenation Reaction in an Organic Solvent Using a Pd/C Catalyst. *Ind. Eng. Chem. Res.* **2019**, *58*, 15162−15172.
(58) Perego, C. Experimental methods in catalytic kinetics. *Catal. Today* **1999**, *52*, 133−145.
(59) Dumesic, J. A.; Huber, G. W.; Boudart, M. *Chemical Engineering: Catalyst Science and Technology*; NPTEL: 2014; pp 1−15.
(60) Singh, U. K.; Vannice, M. A. Kinetics of Liquid-Phase Hydrogenation Reactions over Supported Metal Catalysts. *Appl. Catal., A* **2001**, *213*, 1−24.
(61) Weisz, P. B.; Prater, C. D. Interpretation of Measurements in Experimental Catalysis. *Adv. Catal.* **1954**, *6*, 143−196.
(62) Pintar, A.; Berčič, G.; Levec, J. Catalytic liquid-phase nitrite reduction: kinetics and catalyst deactivation. *AIChE J.* **1998**, *44*, 2280−2292.
(63) Wilke, C. R.; Chang, P. Correlation of diffusion coefficients in dilute solutions. *AIChE J.* **1955**, *1*, 264−270.
(64) Chen, Y.; Miller, D. J.; Jackson, J. E. Kinetics of aqueous-phase hydrogenation of organic acids and their mixtures over carbon supported ruthenium catalyst. *Ind. Eng. Chem. Res.* **2007**, *46*, 3334−3340.
(65) Cheng, S.; Wei, L.; Zhao, X.; Julson, J. Application, Deactivation, and Regeneration of Heterogeneous Catalysts in Bio-Oil upgrading. *Catalysts* **2016**, *6*, 195.
(66) Mortensen, P. M.; Grunwaldt, J. D.; Jensen, P. A.; Knudsen, K. G.; Jensen, A. D. A review of catalytic upgrading of bio-oil to engine fuels. *Appl. Catal., A* **2011**, *407*, 1−19.
(67) Wan, H.; Vitter, A.; Chaudhari, R. V.; Subramaniam, B. Kinetic investigations of unusual solvent effects during Ru/C catalyzed hydrogenation of model oxygenates. *J. Catal.* **2014**, *309*, 174−184.
(68) Maccarrone, M. J.; Torres, G. C.; Lederhos, C.; Betti, C.; Badano, J. M.; Quiroga, M. Kinetic Study of the Partial Hydrogenation of 1-Heptyne over Ni and Pd Supported on Alumina. *Hydrogenation*; Intech: 2012; Chapter 7, pp 159−184.
(69) Svachula, J.; Tichy, J.; Machek, J. Kinetics of hydrogenation of acrylic acid to propionic acid on a copper catalyst. *Appl. Catal.* **1988**, *38*, 53−59.
(70) Bindwal, A. B.; Vaidya, P. D. Kinetics of aqueous-phase hydrogenation of levoglucosan over Ru/C catalyst. *Ind. Eng. Chem. Res.* **2013**, *52*, 17781−17789.
(71) Jain, A. B.; Vaidya, P. D. Kinetics of aqueous-phase hydrogenation of model bio-oil compounds over a Ru/C catalyst. *Energy Fuels* **2015**, *29*, 361−368.

DOI: 10.1021/acs.energyfuels.9b02993
Energy Fuels 2019, 33, 11712−11723